IEEE Photonics Journal
An IEEE Photonics Society Publication

Open Access

Feasibility Study and Experimental Verification of Simplified Fiber-Supported 60-GHz Picocell Mobile Backhaul Links

Volume 5, Number 4, August 2013

Alexander Lebedev
Xiaodan Pang
J. J. Vegas Olmos
Marta Beltrán
Roberto Llorente
Søren Forchhammer
Idelfonso Tafur Monroy

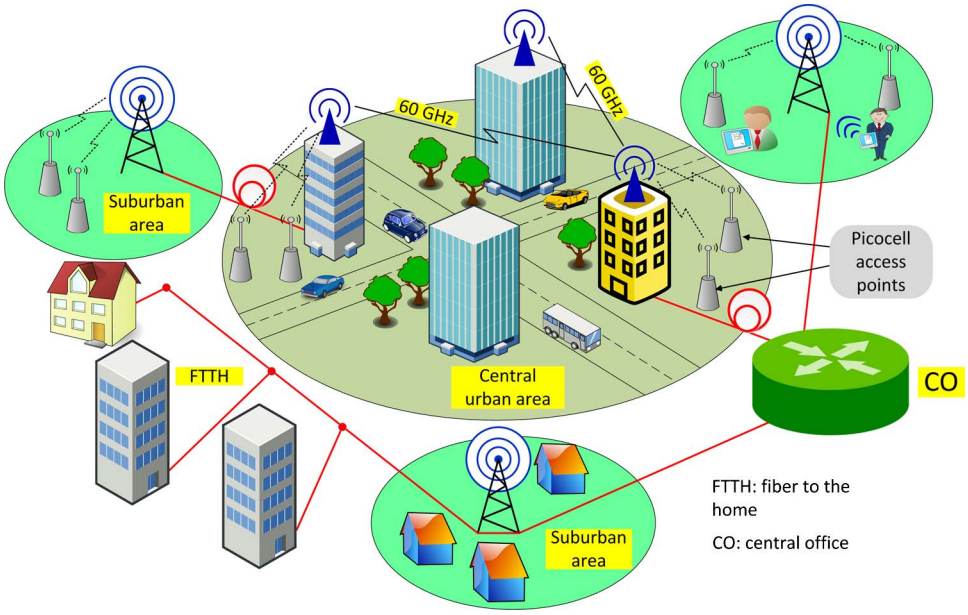

DOI: 10.1109/JPHOT.2013.2277011
1943-0655 © 2013 IEEE

IEEE photonics SOCIETY

IEEE

Feasibility Study and Experimental Verification of Simplified Fiber-Supported 60-GHz Picocell Mobile Backhaul Links

Alexander Lebedev,[1] Xiaodan Pang,[1] J. J. Vegas Olmos,[1] Marta Beltrán,[2] Roberto Llorente,[2] Søren Forchhammer,[1] and Idelfonso Tafur Monroy[1]

[1]DTU Fotonik, Department of Photonics Engineering, Technical University of Denmark, 2800 Kongens Lyngby, Denmark
[2]Valencia Nanophotonics Technology Center, Universidad Politécnica de Valencia, 46022 Valencia, Spain

DOI: 10.1109/JPHOT.2013.2277011

Manuscript received July 5, 2013; revised July 29, 2013; accepted July 30, 2013. Date of current version August 20, 2013. The work of J. J. Vegas Olmos was supported in part by the Marie Curie Program through the WISCON project. M. Beltran and R. Llorente were supported by the Spain National Plan TEC2012-38558-C02-01 MODAL project. Corresponding author: A. Lebedev (e-mail: alele@fotonik.dtu.dk).

Abstract: We propose and experimentally demonstrate a fiber-wireless transmission system for optimized delivery of 60-GHz radio frequency (RF) signals through picocell mobile backhaul connections. We identify advantages of 60-GHz links for utilization in short-range mobile backhaul through feasibility analysis and comparison with an alternative E-band (60–90 GHz) technology. The 60-GHz fiber-wireless-fiber setup is then introduced: two spans of up to 20 km of optical fiber are deployed and bridged by up to 4 m of wireless distance. The 60-GHz radio-over-fiber technology is utilized in the first span of fiber transmission. The system is simplified and tailored for delivery of on-off keying data signals by employing a single module for lightwave generation and modulation combined with a simplified RF downconversion technique by envelope detection. Data signals of 1.25 Gb/s are transmitted, and a bit-error-rate performance below the 7% overhead forward-error-correction limit is achieved for a range of potential fiber deployment scenarios. A spurious free dynamic range of 73 dB-$Hz^{2/3}$ is attained for a frequency-doubling photonic RF upconversion technique. The power budget margin that is required to extend the wireless transmission distance from 4 m to a few hundred meters has been taken into account in the setup design, and the techniques to extend the wireless distance are analyzed.

Index Terms: Microwave photonics, radio over fiber, optical communications.

1. Introduction

Mobile traffic is predicted to grow at a fast pace with video and data communication playing a larger role than voice communication and boosting the capacity requirements [1], [2]. There is a strong demand for larger capacity short range backhaul links supporting picocell connections in dense urban areas [3]. In metropolitan small cell wireless backhaul for picocell wireless networks, the maximum capacity provision is essential, and the cell site spacing is limited to less than 1 km distance [3].

The 60 GHz wireless technology has been already widely adopted by industry for applications such as wireless Gigabit Ethernet bridges reaching distances up to 1 km [4]–[6] and high-definition multimedia interface (HDMI) cable replacement [7]. There is an ongoing research and industrial development in application of the 60 GHz technology for the wireless personal area networking (WPAN) [8], data center interconnects [9]–[11] and mobile backhaul links [12], [13].

Telecommunication services such as broadband compressed and uncompressed high-definition (HD) video transmission in the 60 GHz electrical only [14]–[16] and combined 60 GHz fiber-wireless setups [17]–[22] have been recently reported. Advantages of the 60 GHz links for bandwidth-demanding applications include unlicensed operation in up to 9 GHz of spectrum depending on the national wireless spectrum regulations, availability of narrow-beam compact antennas, and a high level of frequency reuse [23].

Recent industrial reports indicate the rapid progress in the 60 GHz electrical signal generation and component miniaturization [7], [8], [24]. As a result of these developments, there appears also a growing need to transport the RF signals across the optical fiber infrastructure. Photonic RF generation techniques are complementary to electronic techniques and are deployed for low-loss, low electromagnetic interference interconnection of wireless base stations (BS) to the central office (CO) over preexisting fiber infrastructure [25]. The recent development of highly linear high power photoreceivers [26] combining advancements in optoelectronics and mm-wave electronics further strengthens the potential for commercial deployment of 60 GHz fiber-wireless links.

For mm-wave radio transmission, the simplicity and low cost of BS is advantageous as utilization of the mm-wave bands would require a large number of BSs within a small geographical area. In order to simplify the BSs in a network with a fiber connection between the CO and the BS, a radio over fiber (RoF) technology was proposed. In RoF, the BSs are simplified to perform the functions of optical-to-electrical (O/E) conversion, RF amplification and filtering, while expensive mm-wave radio frequency (RF) generation and mixing are avoided at the BSs [27]–[32]. Generation of RoF signals can be performed with diverse optical components [33]–[36] and can be designed transparent to advanced modulation formats [37].

In this paper, we study the application of the 60 GHz wireless technology for providing Gigabit picocell wireless backhaul links fully integrated in a metro/access fiber network. State-of-the-art research on the fiber-wireless mobile backhaul links includes studies on microwave and E-band (60–90 GHz) technologies [38], [39]. In this work, we argue that the deployment of the 60 GHz links for fiber-supported picocell wireless backhaul is beneficial in terms of the link budget, the installation time and the capacity availability for the unlicensed use.

We propose a simplified system in which integrated distributed feedback laser and electro-absorption modulator (DFB-EAM) modules are used for the lightwave generation and data modulation in both RoF and baseband fiber links. It is important to consider the low-cost broad linewidth optical signal generation with a DFB laser in order to tailor the system for simplified on-off keying (OOK) modulation/envelope detection systems suitable for wireless Gigabit backhaul transmission. A broader linewidth of the laser is also reported to increase the threshold for the stimulated Brillouin scattering (SBS) effect [40].

Bit error rate (BER) performance below the 7% overhead forward error correction (FEC) limit for 1.25 Gbps data signal is reported for transmission through a standard single mode fiber (SSMF) link of 20 km, 4 m of wireless distance, and a second span of 20 km SSMF. Given that the wireless distance performance is only tested for up to 4 m because of laboratory space limitations, we propose and analyze methods for further wireless distance extension. In this paper, we significantly extend our work presented in [41] through the report on spurious free dynamic range (SFDR), the feasibility study, updated and extended state-of-the-art in the field and the revised conclusions.

This paper is organized as follows: In Section 2, network architecture of the proposed 60 GHz mobile backhaul system is presented. In Section 3, the feasibility of deployment of 60 GHz links for picocell mobile backhaul connections is analyzed in comparison to the E-band technology. In Section 4, the experimental setup for validation of the proposed architecture is presented. Measurements of the dynamic range of the RoF system in terms of nonlinearities are presented in Section 5. The experimental data are analyzed and the results are discussed in Section 6. Finally, we conclude the paper in Section 7.

2. Network Architecture and Potential Application Scenarios

In densely populated metropolitan areas, deployment of new mobile backhaul connections on a wire becomes prohibitive due to increased installation time and decreased economical feasibility

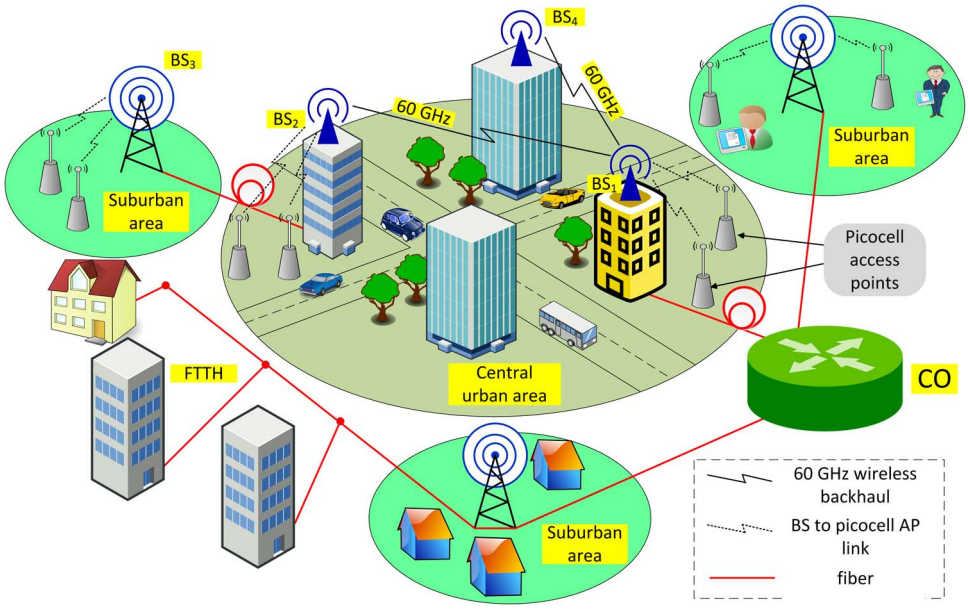

Fig. 1. Network scenario for the 60 GHz urban picocell mobile backhaul link fully supported with a diverse fiber infrastructure. CO: central office, BS: base station, FTTH: fiber to the home. BS_1 and BS_2 operate on the 60 GHz frequency, BS_3 is suggested to operate in the lower frequency licensed bandwidth.

[42]. Contrary to wired solutions, point-to-point mm-wave links can be installed quickly with wireless access points mounted on roofs, walls, or telecommunication poles. As shown in Fig. 1, BS_1-BS_2 link represents the urban mobile backhaul connection. Fiber interface to the BS_1 and the BS_2 provides connection to the CO and the suburban BS_3, respectively. BS_1, BS_2, and BS_4 are supporting multiple urban picocells, and BS_3 is supporting the suburban picocells. By adding a fiber connection from BS_2 to BS_3, a hybrid solution for metropolitan/suburban backhaul of picocell networks is provided.

We employ optical fiber for the RF signal delivery from the CO to the BS_1. The data are then transmitted wirelessly to the BS_2 on the 60 GHz RF carrier. Outside of the central urban area, backhauling is then performed using preexisting optical fiber infrastructure (BS_2-BS_3 connection). The signal arrives to the BS_3 in a baseband format where it can be subsequently upconverted for BS-access point communication.

It is also important to point out that the fiber infrastructure is expected to be shared between baseband digital systems providing broadband fiber-to-the-home (FTTH) services simultaneously with backhaul traffic delivery. This architecture can also be extended to fit the RF generation and delivery in wavelength division multiplexing (WDM) systems [43], [44], enabling simultaneous delivery of the 60 GHz RF carrier in CO-BS_1-BS_2 and CO-BS_1-BS_4 directions.

3. Feasibility Modeling of Wireless Mobile Backhaul Links Transmission in the 60 GHz Band

In this section, we perform a large-scale mm-wave channel modeling in which V (50–75 GHz) and E (60–90 GHz) band line-of-sight (LOS) outdoors RF transmission systems are compared. We argue that the use of the 60 GHz technology is advantageous for the point-to-point picocell mobile backhaul deployment on distances up to a few hundred meters.

Attenuation of the RF signals during air transmission for the LOS outdoors case consists of two major components: the free space path loss and the loss due to atmospheric absorption on molecules of oxygen and water vapor. We place the center frequencies in V- and E-band at the centers of

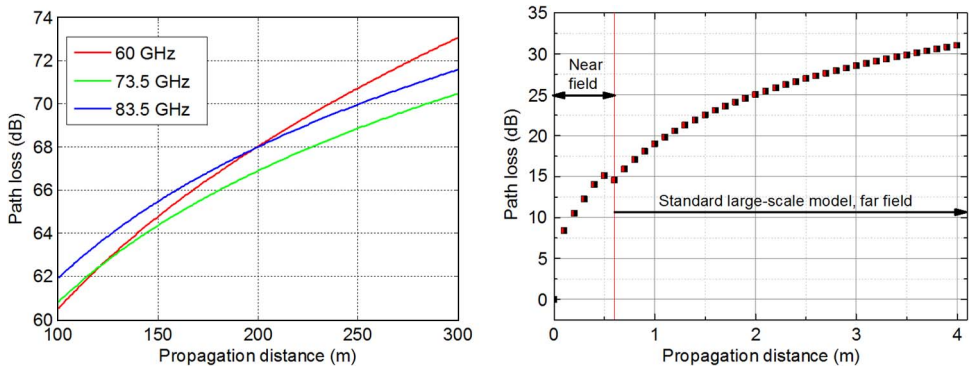

Fig. 2. The combined free space path loss and atmospheric absorption as a function of wireless transmission distance for E- and V-band outdoors links (left) and indoor V-band links (right).

spectrum windows available for unlicensed and 'light licensing' deployment (60 GHz, 73.5 GHz, and 83.5 GHz).

The free space path loss is calculated using the Friis transmission equation. By including the attenuation of the signal related to atmospheric absorption, we arrive to the Eq. (1) for calculation of the path loss for air transmission:

$$\alpha = 20\ log_{10}\left(\frac{4\pi R}{\lambda}\right) + L_{gas} - G_{tx} - G_{rx}, \tag{1}$$

where R (m) is a transmission distance, λ (m) is a wavelength of the signal, L_{gas} (dB) is the atmospheric absorption related attenuation, G_{tx} and G_{rx} are gain of transmitting and receiving antennas respectively (we set these to 25 dBi each). Gaseous attenuation including both water vapor and oxygen-related absorption peaks at the 60 GHz frequency reaching the value of approximately 15 dB/km due to the absorption peak on oxygen molecules, however across E-band combined attenuation on molecules of oxygen and water vapor is measured to be about 0.4 dB/km [45]. In order to compare the performance of V- and E-band systems for wireless distances suitable for dense metropolitan backhaul of picocell networks, we plot the results of numerical calculation for the combined signal attenuation in Fig. 2 (left).

From Fig. 2 (left), it can be seen that the 60 GHz transmission link shows a lower path loss in a range of about 200 m compared to the E-band solution centered at 83.5 GHz and at about 130 meters for 73.5 GHz centered E-band link, the attenuation penalty does not exceed 3 dB in the links up to 300 m. Thus, the 60 GHz links can achieve performance superior/close to the E-band links in the range up to a few hundred meters in terms of added contributions from the free space path loss and atmospheric absorption on the molecules of oxygen and water vapor.

In Fig. 2 (right) the 60 GHz path loss for indoor wireless distances is presented. We have first experimentally measured the RF attenuation in a near-field area where the standard Friis transmission equation does not apply. The Fraunhofer distance defining the border between near- and far-field propagation is calculated according to:

$$d_f = \frac{2D^2}{\lambda}, \tag{2}$$

where D is the largest dimension of an antenna, in our case it is equal to 0.039 m, and λ is a wavelength of the radio signal. The results show a close match around the Fraunhofer distance between experimentally measured values of attenuation in the near field and values calculated according to Eq. (1) in the far field.

Using the Eq. (1), we obtain that, in order to extend the wireless distance from 4 m to 300 m, 42 dB improvement in the electrical link budget is required. It is therefore critical that we design the laboratory setup capable to accommodate this requirement.

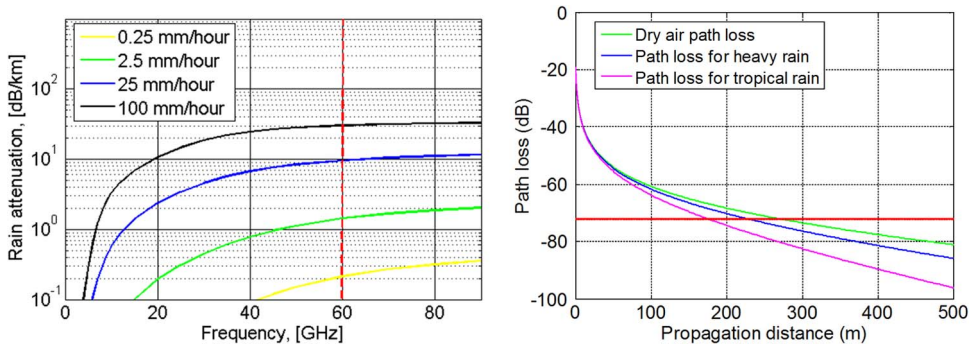

Fig. 3. Rainfall attenuation as a function of frequency (left) and combined path loss and rainfall attenuation for 60 GHz RF propagation versus required SNR level (right) as a function of wireless distance.

Another important performance criterion for wireless communication is stability of the link under the weather influence. In this paper, we analyze the influence of rain on transmission performance. An estimate of the rain attenuation is given by:

$$\gamma_R = kR^{\alpha}, \tag{3}$$

where γ_R (dB/km) is the specific rain-related attenuation, and R (mm/hour) is the rain rate parameter differentiating the intensity of a rainfall. The coefficients k and α are frequency dependent and may be either determined by curve-fitting equations or through a set of specified values given in Recommendation P.838-2 [46]. Rain types are separated as a 'drizzle: 0.25 mm/hour', a 'light rain: 2.5 mm/hour', a 'heavy rain: 25 mm/hour', and a 'tropical rain: 100 mm/hour' [3]. Fig. 3 (left) presents the simulation results based on the recommendation.

60 GHz links have slightly lower rainfall attenuation values compared to E-band links as depicted in Fig. 3 (left). In Fig. 3 (right) we display the effect that the 'heavy' and the 'tropical' rain will have on the operation of the 60 GHz link in terms of shortening the transmission distance for a given signal-to-noise ratio (SNR) required at the receiver. We define the limit on the path loss by the closeness of the 60 GHz RF signal power to the noise floor defined by the Johnson noise. The path loss margin β available for a given requirement on the SNR (we set SNR of 18 dB which for envelope-detected signals yields BER less than 10^{-12}), given bandwidth of the signal $(B = 2.5$ GHz$)$, given RF power before the antenna $(P_{tx} = 10$ dBm$)$ is then equal to:

$$\beta = P_{tx} - 10log_{10}(1000 \times kt) - 10log_{10}(B) - SNR, \tag{4}$$

where k is a Boltzmann's constant, and t (K) is a room temperature. We have calculated β to be equal to 72 dB for our bitrate. The values of path loss are then calculated as a sum of (1) and (3) for antenna gain of 25 dBi. As we see in Fig. 3 (right), the influence of weather conditions shortens the reliable wireless link length, however, in order to combat this, FEC techniques are typically used [4], [6]. It is also clear from Fig. 3 (right) that the reliable link length can be extended by increasing the power at the transmitter or increasing the antenna gain.

Given the modeling results, it is clear that the 60 GHz links are a good solution for the picocell backhaul transmission systems on a distance up to a few hundred meters in terms of combined effects of the free space path loss, the atmospheric absorption and the possible rain attenuation. There are few additional aspects that have to be considered before making a choice between V- or E-band links for deployment in picocell mobile backhaul. First, V-band links provide unlicensed operation, when E-band transmission requires light licensing which may incur additional delays in the link installation time. Second, the current market costs of the equipment based on the V-band technology are lower than that of the E-band links [4]. Last, with a quick reduction of power level when the signal is following other than the LOS path, superior multipath interference immunity and high frequency reuse are enabled for 60 GHz systems.

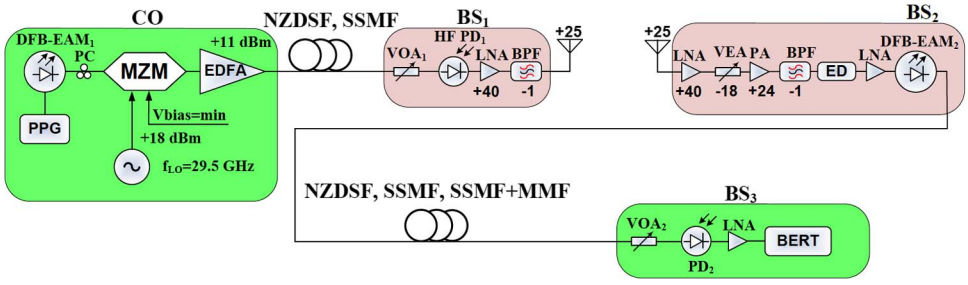

Fig. 4. Laboratory setup for a fiber-wireless-fiber 60 GHz link. DFB-EAM: distributed feedback laser integrated with an electro-absorption modulator, PPG: pulse pattern generator, MZM: Mach-Zehnder modulator, LO: local oscillator, EDFA: Erbium doped fiber amplifier, HF PD: high frequency photodiode, LNA: low noise amplifier, BPF: bandpass filter, VOA: variable optical attenuator, VEA: variable electrical attenuator, PA: power amplifier, ED: envelope detector, BERT: bit error rate tester, CO: central office, BS: base station, SSMF: standard single mode fiber, NZDSF: non-zero dispersion shifted fiber, MMF: multimode fiber.

We believe that the feasibility study presented in this section supports the relevance of studying the 60 GHz links for picocell mobile backhaul. In the next sections, a simplified 60 GHz fiber-wireless-fiber setup is built, and its performance is characterized experimentally.

4. Experimental Setup Description

The schematics of the experimental setup of the 60 GHz fiber-wireless picocell mobile backhaul link including two spans of fiber and a single 60 GHz wireless link in between is presented in Fig. 4. Four subsystems are emulated: a CO transmitter and three BSs (BS_1-BS_3). RoF generation and data modulation are located at the CO; BS_1 performs the O/E conversion and amplifies the 60 GHz RF signal before the radiation, BS_2 performs the RF downconversion and remodulation onto the lightwave. BS_3 recovers the original baseband data by O/E conversion.

A DFB-EAM module was used to produce a lightwave at a wavelength $\lambda = 1550$ nm with 4 dBm of optical power. A 1.25 Gbps nonreturn to zero (NRZ) pseudorandom binary sequence (PRBS) with a word length of $2^{15} - 1$ generated by a pulse pattern generator (PPG) was directly modulated onto the lightwave at the DFB-EAM_1. The use of the DFB-EAM for lightwave generation and data modulation relaxes requirements for a peak-to-peak voltage of the electrical signal driving the modulator and simplifies the overall system installation. Chirp effects common to EAM technology were controlled through application of an optimal voltage.

RF modulation of the lightwave was performed using a single-drive Mach-Zehnder modulator (MZM). A polarization controller (PC) was placed before the MZM in order to minimize the polarization-dependent loss. The MZM was biased at a minimum transmission point and driven by a high-power sinusoidal local oscillator (LO) RF $(+18\ \text{dBm}, f_{LO} = 29.5\ \text{GHz})$, resulting in a suppression of the original optical carrier and increase of optical power in upper and lower sidebands separated by twice the original RF frequency $2f_{LO}$. This technique for generation of RoF signals is known as an optical carrier suppression (OCS) technique [47]. By using the OCS method, the requirements for high frequency RF components at the CO are alleviated, and high quality phase noise performance is obtained due to the fact that upper and lower sidebands are produced by the same laser. The optical spectrum of the generated double-sideband with a suppressed carrier (DSB-SC) signal is presented in Fig. 5 (left). A suppression of the optical carrier relative to the RF-produced sidebands of approximately 20 dB was achieved constrained by both the polarization alignment and the extinction ratio of the modulator.

The signal was subsequently coupled into an Erbium doped fiber amplifier (EDFA) in order to improve the power budget before the launch into the fiber. Subsequently, fiber transmission was performed through SSMF and non-zero dispersion shifted fiber (NZDSF). We detected the electrical RF signal through photomixing at a 75 GHz bandwidth p-i-n photodiode (PD_1). The variable optical attenuator (VOA_1) was placed before the PD_1 in order to control the power entering the PD_1. After

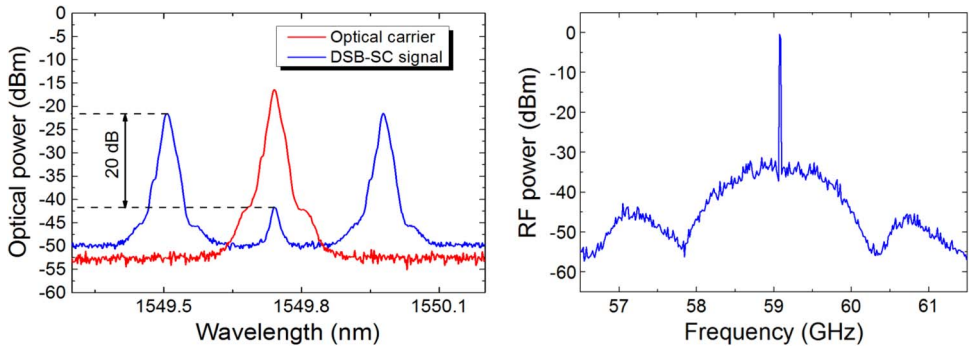

Fig. 5. Optical spectra of the transmitted signal (left) and RF spectrum of the signal before radiation (right).

photomixing, the 60 GHz RF signal was amplified with a 40 dB gain double-stage low noise amplifier (LNA), passed through a bandpass filter and radiated with a horn antenna (+25 dBi gain). The spectrum of the modulated RF signal is depicted in Fig. 5 (right). The path loss for 4 m wireless distance including the combined gain of antennas (50 dBi) is equal to approximately 31 dB which was calculated using the Eq. (1) presented in Section 3. The equivalent omnidirectional path loss (antenna gain is excluded) is equal to 81 dB.

After reception with an equivalent antenna, the signal was amplified with a 40 dB gain LNA. We have then employed a variable electrical attenuator (VEA) and a power amplifier (PA) in order to emulate the effect of the possible wireless distance extension on the system performance. The VEA has been set to attenuate the signal by 18 dB throughout the measurements. The signal was then filtered and the data signal were downconverted from RF into baseband at a zero-biased Schottky diode serving as an envelope detector (ED). We refer the readers to [48] for a thorough study on basic principles of Schottky diodes' operation. Main advantage of the envelope detection technique is that it allows performing the RF signal downconversion without using an RF LO and a phase locked loop circuitry required for the synchronous mixing detection technique. Following the ED, the signal was amplified to bring the peak-to-peak voltage level of the signal to a value required for effective driving of the DFB-EAM$_2$.

After the subsequent remodulation on the lightwave, the signal was passed through diverse types of optical fiber. We have included multimode fiber (MMF) in a second span of fiber transmission in order to address the fiber distribution in network connections where the metro/access delivery is integrated with MMF-wired local area network (LAN) distribution. The baseband electrical data were finally recovered with a 10 GHz bandwidth p-i-n PD. After amplification, it was fed to a BER tester (BERT) for further signal quality evaluation.

5. Characterization of the SFDR

An SFDR measurement is needed in order to quantify performance of the RoF system in terms of nonlinearities of link components, i.e. appearance of spurious harmonics of the RF signal that are located in the bandwidth of data modulation and contribute to BER deterioration. The SFDR of the system is the range between the smallest signal that can be transmitted and received by the system and the largest signal that can be introduced into the system without creating distortions above the noise floor after detection in the bandwidth of interest [49]. SFDR gives better system performance estimate than maximum achievable SNR which is constrained by noise floor and saturation only. Given that in order to extend the wireless link distance for outdoor scenarios we need to improve the power budget, we have measured the SFDR including EDFA and increased optical power into the PD.

In Fig. 6, we present the setup for measuring the SFDR of the modulation and upconversion block in the system. We built the SFDR setup based on a part of the general setup—a link between the CO and the BS$_1$. The signal is then analyzed directly on the output of the PD.

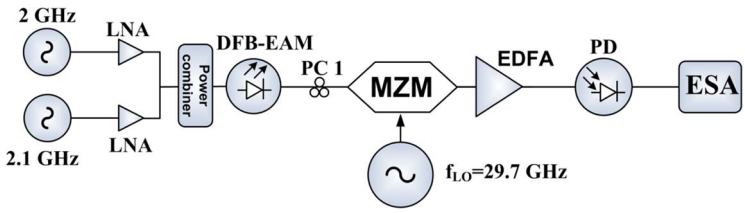

Fig. 6. Laboratory setup for measuring SFDR. LNA: low noise amplifier, DFB-EAM: distributed feedback laser integrated with electro absorption modulator, PC: polarization controller, LO: local oscillator, MZM: Mach-Zehnder modulator, EDFA: Erbium doped fiber amplifier, PD: photodiode, ESA: electrical spectrum analyzer.

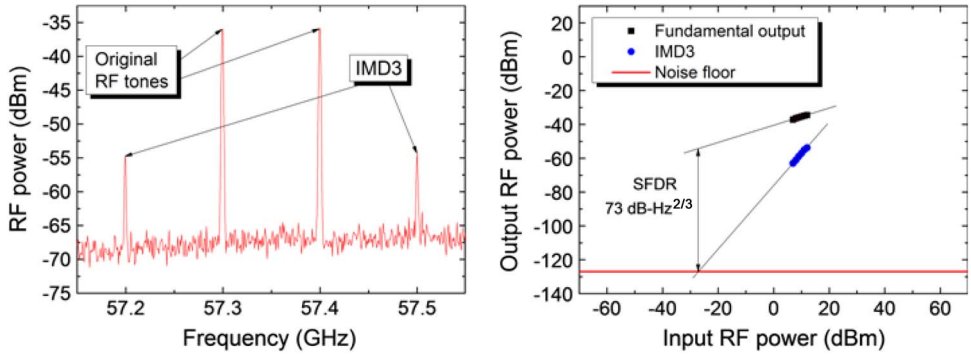

Fig. 7. SFDR measurement for a chosen RF generation technique.

Two RF tones modulating the DFB-EAM were located at 2 GHz (f_1) and 2.1 GHz (f_2) RF frequency; the f_{LO} was set to 29.7 GHz. According to [49], third order intermodulation (IMD3) components are expected to be located at 59.4 GHz $+ 2 \times f_1 - f_2 = 57.5$ GHz and 59.4 GHz $+ 2 \times f_2 - f_1 = 57.2$ GHz. Fig. 7 (left) shows the RF spectra including the original RF tones and IMD3 tones. The optical power at the PD was set to 5 dBm throughout the SFDR measurement. It should be noted that the SFDR was measured for a transmitter including EDFA, which increases the noise level at the PD, but gives characterization of the system suitable for extended optical and wireless transmission.

Increasing RF power modulating the lightwave improves the SNR, however, the IMD3 distortion is increasing at a faster rate than the signal. As seen in Fig. 7 (right), we achieved the SFDR value of 73 dB-Hz$^{2/3}$ that is comparable to results obtained by other authors who use similar frequencies of two RF tones [50]. The obtained value of SFDR provides sufficient margin in terms of nonlinearity and sets the limit on system's scalability for a range of RF powers to be transmitted through the optical fiber.

We have reported on SFDR of the system for increased shot noise (by setting the optical power into the PD to +5 dBm) and included EDFA. EDFA deployment is reported to decrease the SFDR value of the system [49], but it is a necessity in order to improve the power budget for fiber-wireless reach extension. By setting maximum constraints to SFDR, we present the limit on the system performance.

6. Results and Discussion

In this section, we describe the setup performance under a constraint of decreasing optical power on the output of the second span of optical fiber transmission; at the same time, optical power impinging the PD_1 is kept constant at -7 dBm. The curve depicting the generated 60 GHz RF power as a function of carrier suppression is measured to support the link budget discussion. The phase noise performance of the photonically generated RF carrier is also analyzed including

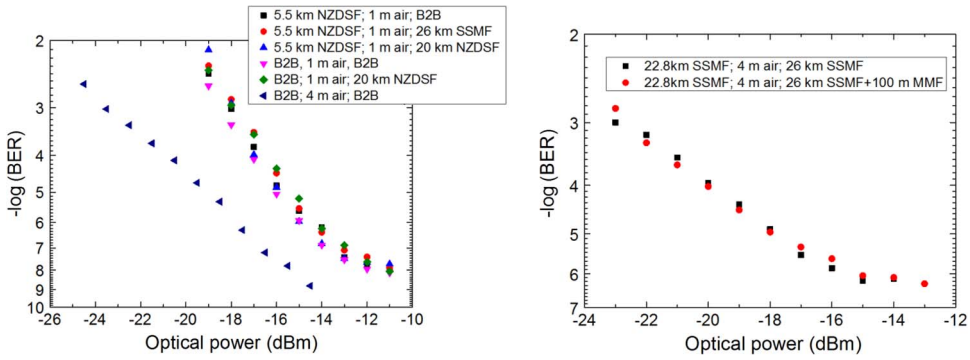

Fig. 8. BER as a function of optical power measured at the PD_2 for B2B/5.5 km NZDSF (left) and 22.8 km SSMF (right) of fiber distance in the first span.

measurements for different types of optical fiber in the first fiber transmission span. BER has been used as a main criterion of system performance constrained by the values of optical power impinging the PD_2, the length of fiber and the wireless transmission distance.

First, we present the results with relaxed requirements for the first span of fiber transmission in terms of dispersion in Fig. 8 (left). We transmit the signal back-to-back (B2B) or employ 5.5 km NZDSF in the first fiber span of the setup and fiber of different lengths and types in the second span. Fig. 8 (left) shows that deployment of SSMF and NZDSF in the second span of transmission introduces no penalty compared to B2B case; however, in all three cases of fiber deployment (B2B, SSMF, NZDSF) in the second span, we observed an error floor on BER performance at approximately 10^{-8} level for 1 m of wireless distance. We suggest that the error floor is not related to chromatic dispersion (CD) given that the distortion of 60 GHz RoF 1.25 Gbps data signal due to CD can be considered negligible in 5.5 km NZDSF and absent in B2B transmission case. We suggest that the error floor is therefore related to degradation of the SNR in the system and to the modulation efficiency of the DFB-EAM_2 which depends on the peak-to-peak voltage level of the baseband electrical signal recovered with ED. Optical B2B curve for 4 m wireless distance in Fig. 8 (left) indicates that, by extending the wireless distance, we are improving the DFB-EAM_2 modulation performance, and the error floor is avoided for extended wireless distances for the same SNR before remodulation on the lightwave. We therefore conclude that presence of the error floor is not related to performance of the wireless channel, i.e. only extension of the wireless distance, and can be mitigated by installing an automatic level control circuit before remodulation on the DFB-EAM_2 to preserve high modulation efficiency and avoid overmodulation.

We then proceeded to emulate deployment of larger distances of fiber in the first span of transmission. Fig. 8 (right) indicates that, when we deploy about 20 km of fiber in both spans, an error floor is present at about a 10^{-6} level. Presence of an error floor is now related to CD impairing the signal in the first span of transmission. When two sidebands are photomixed at the PD, the signal suffers from intersymbol interference caused by a delay between the pulses transmitted on upper and lower sidebands which is reported as a 'bit walk-off' in [51]. However, the periodic dispersion-induced RF power fading is eliminated when the optical carrier is suppressed [51]. For both 1 m and 4 m wireless transmission cases employing fibers with different values of dispersion (NZDSF, SSMF), we demonstrate BER performance well below the 2×10^{-3} limit corresponding to a 7% FEC overhead. BER degradation due to the time shifting of the pulses in the upper and lower sidebands in the first fiber span can be overcome by using a single sideband modulation or diverse CD compensation techniques, however this would increase the setup complexity. Overall, considering the original goal of building a simplified setup, the fact that the penalty is also related to multiple noise sources, and the fact that the FEC is typically implemented in the 60 GHz links [4], [6], we believe that our setup will be a suitable solution for simplified fiber-supported 60 GHz picocell mobile backhaul links.

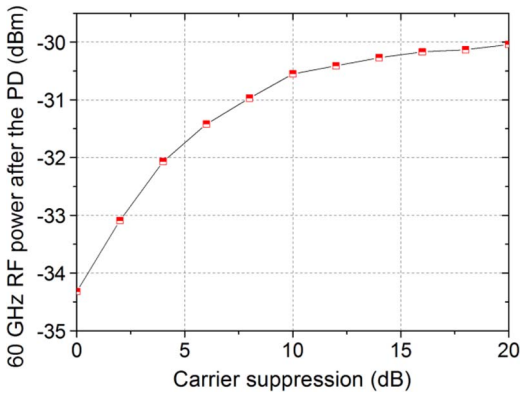

Fig. 9. 60 GHz RF power on the PD output as a function of carrier suppression of the DSB-SC signal.

We have investigated SSMF deployment interfaced with MMF (Fig. 8, right), an appropriate scenario for this combination will be the interface between the access network deployed using SSMF and LAN using MMF. Lightwave was centrally launched from SSMF into MMF which enables mode filtering by exciting only a limited number of lower order modes in the MMF [52]. Intermodal dispersion is thus mitigated because in this case coupling between high and low order modes is reduced significantly. On the receiving side, MMF has been interfaced to the PD by a short patchcord of SSMF (used 75 GHz bandwidth PD only had the SSMF interface) by using which we recover the lowest-order mode (LP_{01}) which implies higher power loss on coupling from MMF to SSMF.

RoF systems in general suffer from the high loss on O/E and E/O conversion due to the resistive impedance matching being an issue at both the transmitter and the receiver. In Fig. 9, we depict power of the 60 GHz RF signal as a function of the sideband-to-carrier suppression ratio which was varied by applying a changing bias voltage. As depicted in Fig. 9, in our system, high power 30 GHz RF signal ($+18$ dBm) applied at the E/O conversion point is subsequently recovered after photomixing as a -30 dBm 60 GHz RF signal for optimized value of 20 dB carrier suppression and a fixed PD_1 input optical power of 0 dBm. 1 dB reduction in optical power entering the PD will result in 2 dB reduction in the 60 GHz RF power. Thus, at -7 dBm optical power entering the PD, RF at the PD output will be equal to -44 dBm.

In order to extend the wireless link length from 4 m to 300 m of wireless distance, we have to address the necessary provision of 42 dB power margin compared to the link budget of 4 m wireless distance as calculated in Section 3. There are few generally applied techniques to improve the electrical link budget and increase the wireless transmission distance. First, a common technique is to use antennas of higher gain. For V-band, antennas of 42 dBi gain are commercially available which may simultaneously add 34 dB to a power budget of the link. Second, the link distance can be extended through amplification. VEA-PA combination that we employ at the BS_2 may be adjusted to bring the additional 18 dB power without introduction of noise by setting the VEA attenuation to 0. The noise figure of the PA is already a part of the link impairments. Depending on link design, PA might be also offset to the transmitting side. These two methods combined bring a gain of 52 dB to the link that surpasses the required margin of 42 dB. However, it must be taken into account for the link design that, when employing a higher gain antenna, the Fraunhofer distance will increase. For a commercially available lens horn antenna of 42 dBi gain with a diameter of 0.25 m, the Fraunhofer distance is equal to 25 m.

In this work, we study transmission of the OOK signals. However, transparency for higher order modulation formats is an important design criterion for RoF links. High performance of the RF oscillator in terms of phase noise is required to enable such transparency. DSB-SC RoF setups are known to have an excellent performance in terms of phase noise because the sidebands are produced by the same laser source and thus are correlated with each other. We depict the phase

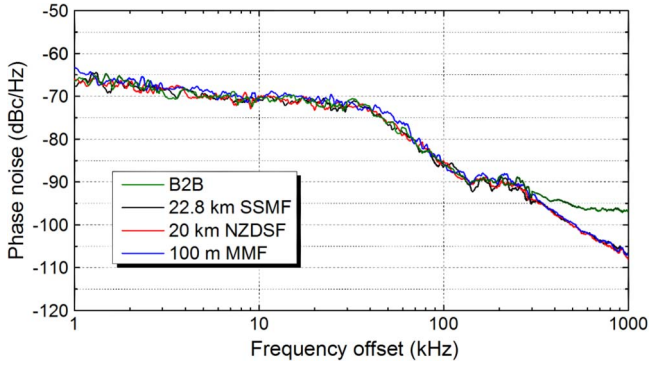

Fig. 10. Phase noise of photonically generated 60 GHz RF signals.

noise performance of the 60 GHz signal before radiation in Fig. 10. We observe a negligible difference in the RF phase noise for generation of the signals that employ different types of fiber benchmarked against B2B optical transmission with the phase noise approximately equal to −85 dBc/Hz at a 100 kHz offset. We conclude that fiber transmission in our setup does not deteriorate the RF phase noise performance. The setup performance is therefore constrained with the phase noise degradation due to multiplication only [53]. In order to enable the higher spectral and power efficiency modulation formats, synchronous downconversion of the RF-modulated signal has to be performed such as in [20] and [54].

7. Conclusion

We experimentally demonstrate the 60 GHz fiber-wireless-fiber communication system enabling the Gigabit picocell mobile backhaul links. Suitability of the proposed approach to diverse fiber deployment scenarios has been assessed. BER performance below the 7% overhead FEC limit is reached for 1.25 Gbps data signals transmission through up to 4 m wireless distance and up to 20 km of SSMF interfacing transmitting and receiving 60 GHz BSs. We simplify the system through the use of the integrated DFB-EAM module in both fiber spans of transmission. The system is further simplified through the use of the ED RF detection technique achieving passive downconversion and eliminating the need for the design of synchronization hardware. 73 dB-$Hz^{2/3}$ SFDR is reported when the EDFA is included as a part of an optical transmitter. Phase noise performance indicates high potential of the system for transmission of advanced modulation formats. Future work is directed towards combating the error floor in the system which will include the fiber-wireless-fiber transmission when RF is generated through photomixing of lightwaves produced by two free running lasers. We suggest that the work can be extended by direct comparison of experimental performance of V- and E-band systems and the SFDR measurement for the link including fiber transmission.

Acknowledgment

The authors would like to acknowledge the support from Radiometer Physics GmbH for loan of V-band amplifiers.

References

[1] Cisco white paper, "Cisco visual networking index: Global mobile data traffic forecast update, 2012–2017" 2012. [Online]. Available: http://www.cisco.com/en/US/solutions/collateral/ns341/ns525/ns537/ns705/ns827/white_paper_c11-520862.pdf
[2] Traffic and market data report, Ericsson, Stockholm, Sweden, 2011, Ericsson white paper.
[3] J. Wells, *Multi-Gigabit Microwave and Millimeter-Wave Wireless Communications*. Norwood, MA, USA: Artech House, 2010.
[4] Gigabit wireless applications using 60 GHz radios, Bridgewave, Santa Clara, CA, USA, 2006, Bridgewave whitepaper.

[5] A. Mathew, *Local Area Networking Using MillimetreWaves*. Acton, MA, USA: NewLANs, Inc., 2005.
[6] AIRLINX Communications, Inc. specification datasheet, "GigaLink 6221/6421/6451" 2013, (AIRLINX Communications, Inc.).
[7] *WirelessHD Specification Version 1.1 Overview*, WirelessHD, Morgan Hill, CA, USA, 2010, WirelessHD white paper.
[8] WiGig white paper, Defining the future of multi-gigabit wireless communication, Jul. 2010, (WiGig alliance).
[9] K. Ramachadran, R. Kokku, R. Mahindra, and S. Rangarajan, "60 GHz data-center networking: Wireless worry less?" NEC, Princeton, NJ, USA, Tech. Rep., 2008.
[10] S. Kandula, J. Padhye, and P. Bahi, "Flyways to de-congest data center networks," in *Proc. 8th ACM Workshop Hot Topics Netw.*, 2009, pp. 1–6.
[11] K. Kawasaki, Y. Akiyama, K. Komori, M. Uno, H. Takeuchi, T. Itagaki, Y. Hino, Y. Kawasaki, K. Ito, and A. Hajimiri, "A millimeter-wave intra-connect solution," in *Proc. IEEE Int. Solid-State Circuits Conf.*, 2010, pp. 414–415.
[12] Ceragon application note, Wireless backhaul solutions for small cells, (Ceragon).
[13] Sub10 Systems Limited White Paper, "60GHz metro cell and small cell backhauling for service providers," 2011, (Sub10 Systems Limited).
[14] H. Singh, J. Oh, C. Kweon, X. Qin, H. Shao, and C. Ngo, "A 60 GHz wireless network for enabling uncompressed video communication," *IEEE Commun. Mag.*, vol. 46, no. 12, pp. 71–78, Dec. 2008.
[15] Z. Lan, J. Wang, C.-S. Sum, T. Baykas, C. Pyo, F. Kojima, H. Harada, and S. Kato, "Unequal error protection for compressed video streaming on 60 GHz WPAN system," in *Proc. Int. Wireless Commun. Mobile Comput. Conf.*, 2008, pp. 689–693.
[16] H. Singh, X. Qin, H. Shao, C. Ngo, C. Kwon, and S. S. Kim, "Support of uncompressed video streaming over 60 GHz wireless networks," in *Proc. 5th IEEE Consum. Commun. Netw. Conf.*, 2008, pp. 243–248.
[17] A. Chowdhury, H.-C. Chien, Y.-T. Hsueh, and G.-K. Chang, "Advanced system technologies and field demonstration for in-building optical-wireless network with integrated broadband services," *J. Lightw. Technol.*, vol. 27, no. 12, pp. 1920–1927, Jun. 2009.
[18] A. Lebedev, T. T. Pham, M. Beltrán, X. Yu, A. Ukhanova, R. Llorente, and I. Tafur Monroy, "Optimization of high-definition video coding and hybrid fiber-wireless transmission in the 60 GHz band," *Opt. Exp.*, vol. 19, no. 26, pp. 895–904, Dec. 2011.
[19] A. Lebedev, J. J. Vegas Olmos, X. Pang, S. Forchhammer, and I. Tafur Monroy, "Demonstration and comparison study for V- and W-band real-time high-definition video delivery in diverse fiber-wireless infrastructure," *Fiber Integr. Opt.*, vol. 32, no. 2, pp. 93–104, 2013.
[20] A. Lebedev, J. J. Vegas Olmos, M. Iglesias, S. Forchhammer, and I. T. Monroy, "Enabling uncompressed video transmission in double-sideband 60 GHz radio-over-fiber links," in *Proc. IEEE IPC*, 2012, pp. 578–579, Paper WS2.
[21] Z. Tang and S. Pan, "Transmission of 3-Gb/s uncompressed HD video in a optoelectronic-oscillator-based radio over fiber link," in *Proc. IEEE 13th Topical Meet. SiRF*, 2013, pp. 219–221.
[22] J. Guillory, A. Pizzinat, P. Guignard, F. Richard, B. Charbonnier, P. Chanclou, and C. Algani, "Simultaneous implementation of gigabit Ethernet, RF TV and radio mm-wave in a multiformat home area network," presented at the 37th Eur. Conf. Exhibition Optical Communication (ECOC), Geneva, Switzerland, 2011, Paper We.7.C.3.
[23] S.-K. Yong, *60 GHz Technology for Gbps WLAN and WPAN: From Theory to Practice*. Hoboken, NJ, USA: Wiley, 2011.
[24] Siversima application note, "58–63 GHz V-band converter," 2013, (Siversima).
[25] C. Lim, A. Nirmalathas, M. Bakaul, P. Gamage, K.-L. Lee, Y. Yang, D. Novak, and R. Waterhouse, "Fiber-wireless networks and subsystem technologies," *J. Lighwave Technol.*, vol. 28, no. 4, pp. 390–405, Feb. 2010.
[26] S. Fedderwitz, C. Leonhardt, J. Honecker, P. Muller, and A. Steffan, "A high linear and high power photoreceiver suitable for analog applications," in *Proc. IEEE IPC*, 2012, pp. 308–309, Paper TuL3.
[27] K. Xu, X. Sun, J. Yin, H. Huang, J. Wu, X. Hong, and J. Lin, "Enabling ROF technologies and integration architectures for in-building optical–wireless access networks," *IEEE Photon. J.*, vol. 2, no. 2, pp. 102–112, Apr. 2010.
[28] A. Kanno, P. T. Dat, T. Kuri, I. Hosako, T. Kawanishi, Y. Yoshida, Y. Yasumura, and K. Kitayama, "Coherent radio-over-fiber and millimeter-wave radio seamless transmission system for resilient access networks," *IEEE Photon. J.*, vol. 4, no. 6, pp. 2196–2204, Dec. 2012.
[29] X. Zhang, B. Hraimel, and K. Wu, "Breakthroughs in optical wireless broadband access networks," *IEEE Photon. J.*, vol. 3, no. 2, pp. 331–336, Apr. 2011.
[30] X. Li, J. Yu, Z. Dong, and N. Chi, "Photonics millimeter-wave generation in the E-band and bidirectional transmission," *IEEE Photon. J.*, vol. 5, no. 1, p. 7 900 107, Feb. 2013.
[31] A. M. Zin, M. S. Bongsu, S. M. Idrus, and N. Zulkifli, "An overview of radio-over-fiber network technology," in *Proc. IEEE Int. Conf. Photon.*, 2010, pp. 1–3, Paper ICP2010-85.
[32] M. C. Parker, S. D. Walker, R. Llorente, M. Morant, M. Beltran, I. Möllers, D. Jäger, C. Vazquez, D. Montero, I. Libran, S. Mikroulis, S. Karabetsos, and A. Bogris, "Radio-over-fibre technologies arising from the building the future optical network in Europe (BONE) project," *IET Optoelectron.*, vol. 4, no. 6, pp. 247–259, Dec. 2010.
[33] M. Beltrán, J. B. Jensen, R. Llorente, and I. Tafur Monroy, "Experimental analysis of 60-GHz VCSEL and ECL photonic generation and transmission of impulse-radio ultra-wideband signals," *IEEE Photon. Technol. Lett.*, vol. 23, no. 15, pp. 1055–1057, Aug. 2011.
[34] X. Pang, M. Beltrán, J. Sánchez, E. Pellicer, J. J. Vegas Olmos, R. Llorente, and I. Tafur Monroy, "DWDM fiber-wireless access system with centralized optical frequency comb-based RF carrier generation," presented at the Conf. Optical Fiber Communication, Nat. Fiber Optic Engineers Conf., Anaheim, CA, USA, 2013, Paper JTh2A.56.
[35] X. Pang, A. Caballero, A. Dogadaev, V. Arlunno, L. Deng, R. Borkowski, J. S. Pedersen, D. Zibar, X. Yu, and I. Tafur Monroy, "25 Gbit/s QPSK hybrid fiber-wireless transmission in the W-band (75–110 GHz) with remote antenna unit for in-building wireless networks," *IEEE Photon. J.*, vol. 4, no. 3, pp. 691–698, Jun. 2012.
[36] X. Pang, X. Yu, Y. Zhao, L. Deng, D. Zibar, and I. Tafur Monroy, "Experimental characterization of a hybrid fiber-wireless transmission link in the 75 to 110 GHz band," *Opt. Eng.*, vol. 51, no. 4, pp. 045004-1–045004-5, Apr. 2012.

[37] A. Caballero, D. Zibar, R. Sambaraju, J. Martí, and I. T. Monroy, "High-capacity 60 GHz and 75–110 GHz band links employing all-optical OFDM generation and digital coherent detection," *J. Lighwave Technol.*, vol. 30, no. 1, pp. 147–155, Jan. 2012.
[38] T. P. McKenna, J. A. Nanzer, M. L. Dennis, and T. R. Clark, "Fully fiber-remoted 80 GHz wireless communication with multi-subcarrier 16-QAM," in *Proc. IEEE IPC*, 2012, pp. 576–577, Paper WS1.
[39] G. Shen, R. S. Tucker, and C.-J. Chae, "Fixed mobile convergence architectures for broadband access: Integration of EPON and WiMAX," *IEEE Commun. Mag.*, vol. 45, no. 8, pp. 44–50, Aug. 2007.
[40] M. Sauer, A. Kobyakov, and A. B. Ruffin, "Radio-over-fiber transmission with mitigated stimulated Brillouin scattering," *IEEE Photon. Technol. Lett.*, vol. 19, no. 19, pp. 1487–1489, Oct. 2007.
[41] A. Lebedev, X. Pang, J. J. Vegas Olmos, M. Beltran, R. Llorente, S. Forchhammer, and I. Tafur Monroy, "Fiber-supported 60 GHz mobile backhaul links for access/metropolitan deployment," in *Proc. ONDM*, 2013, pp. 190–193.
[42] SKYFIBER whitepaper, "Breaking the backhaul bottleneck: How to meet your backhaul capacity needs while maximizing revenue," 2012, (SKYFIBER).
[43] J. Yu, Z. Jia, L. Yi, Y. Su, G.-K. Chang, and T. Wang, "Optical millimeter-wave generation or up-conversion using external modulators," *IEEE Photon. Technol. Lett.*, vol. 18, no. 1, pp. 265–267, Jan. 2006.
[44] K. Kojucharow, M. Sauer, H. Kaluzni, D. Sommer, F. Poegel, W. Nowak, A. Finger, and D. Ferling, "Simultaneous electrooptical upconversion, remote oscillator generation, and air transmission of multiple optical WDM channels for 60-GHz high-capacity indoor system," *IEEE Trans. Microw. Theory Tech.*, vol. 47, no. 12, pp. 2249–2256, Dec. 1999.
[45] ITU-R P.676-9 Recommendation (2012) Attenuation by atmospheric gases.
[46] ITU-R P.838-2 Recommendation (2003) Specific attenuation model for rain for use in prediction methods.
[47] J. J. O'Reilly, P. M. Lane, R. Heidemann, and R. Hofstetter, "Optical generation of very narrow linewidth millimeter wave signals," *Electron. Lett.*, vol. 28, no. 25, pp. 2309–2311, Dec. 1992.
[48] Skyworks application noteMixer and detector diodes," 2008, (Skyworks).
[49] C. H. Cox, *Analog Optical Links*. New York, NY, USA: Cambridge Univ. Press, 2004.
[50] C. S. Park, Y.-K. Yeo, and L. C. Ong, "Demonstration of the GbE service in the converged radio-over-fiber/optical networks," *J. Lighw. Technol.*, vol. 28, no. 16, pp. 2307–2314, Aug. 2010.
[51] C. Lim, K.-L. Lee, A. Nirmalathas, D. Novak, and R. Waterhouse, "Impact of chromatic dispersion on 60 GHz radio-over-fiber transmission," in *Proc. 21st Annu. Mee. IEEE Lasers Electro-Optics Soc.*, 2008, pp. 89–90, Paper MJ5.
[52] I. Gasulla and J. Capmany, "1 Tb/s·km multimode fiber link combining WDM transmission and low-linewidth lasers," *Opt. Exp.*, vol. 16, no. 11, pp. 8033–8038, May 2008.
[53] G. Qi, J. Yao, J. Seregelyi, and S. Paquet, "Phase-noise analysis of optically generated millimeter-wave signals with external optical modulation techniques," *J. Lighw. Technol.*, vol. 24, no. 12, pp. 4861–4875, Dec. 2006.
[54] A. Lebedev, J. J. Vegas Olmos, M. Iglesias, S. Forchhammer, and I. TafurMonroy, "A novel method for combating dispersion induced power fading in dispersion compensating fiber," *Opt. Exp.*, vol. 21, no. 11, pp. 13 617–13 625, Jun. 2013.